Charge Transfer Interactions of *N*-(4-Carboxyphenyl)trimellitimide Dibutyl Ester

C. Spies,* A. Lorenc, and R. Gehrke

Hamburger Synchrotronstrahlungslabor HASYLAB at Deutsches Elektronensynchrotron DESY, Notkestr. 85, 22603 Hamburg, Germany

H. R. Kricheldorf

Institut für Technische und Makromolekulare Chemie, Universität Hamburg, Bundesstr. 45, 20146 Hamburg, Germany

Received: July 8, 2002; In Final Form: October 16, 2002

Charge transfer (CT) interactions of the dibutyl ester of *N*-(4-carboxyphenyl)trimellitimide (NCTD) dissolved in organic solvents have been investigated by means of UV absorption and fluorescence spectroscopy and time-resolved fluorescence measurements. The spectroscopic data are interpreted in connection with quantum mechanical calculations using the AM1 and ZINDO/S method. The electronic transition lowest in energy, observed as an absorption tail in the UV spectra, is interpreted as a direct intramolecular CT excitation from the *N*-(4-carboxyphenyl) moiety (donor) to the trimellit moiety (acceptor). Independent of the excitation wavelength, a dominant red-shifted CT emission is observed in the fluorescence spectra. Thus, in addition to the direct CT excitation, indirect methods of CT formation exist. In concentrated solutions ground-state stable dimer formation is observed. Direct monomeric CT excitation and ground-state stable dimer excitation takes place in an overlapping energy range. The ground-state stable dimer fluorescence appears blue-shifted with respect to the monomeric CT fluorescence. Ground-state stable dimers exist that have decay times longer than those of the monomeric CT species. As a distribution of decay times is observed in the fluorescence decay curves, dimers with different decay times exist. According to the performed quantum mechanical calculations, dimers with intermolecular CT character are formed.

Introduction

Investigations of CT interactions in *N*-(4-carboxyphenyl)-trimellitimide dibutyl ester (NCTD) have been performed as it serves as a model compound for a repeating part of poly(ester imides).[1] Polyimides are polymers with valuable properties, e.g., high thermal stability and good mechanical behavior.[2] It is still under discussion how the thermal stability and the mechanical properties are influenced or caused by intermolecular CT complex formation.[2] These intermolecular complexes might also promote the formation of liquid crystalline phases in poly(ester imides).[1] As poly(ester imides) and copoly(ester imides) contain several aromatic units in the polymer chain, different intermolecular complex formations are thinkable. To obtain information about possible complex formations, low molecular weight model substances have to be synthesized. In this paper we report about the CT interactions of the dibutyl ester of *N*-(4-carboxyphenyl)-trimellitimide. The chemical structure is shown in Figure 1. The comparably large butyl end group was chosen to increase the solubility of *N*-(4-carboxyphenyl)trimellitimide and because this model substance represents a repeating unit in certain LC-poly-(ester imides).[3] The improved solubility enables to investigate dimer formation in solution, which was observed by fluorescence measurements. To recognize dimer formation, the spectroscopic behavior of the monomer has to be characterized previously. This was performed by spectroscopic measurements on dilute solutions in combination with quantum mechanical calculations.

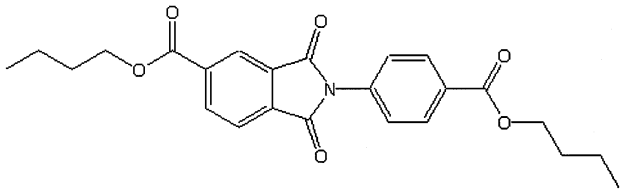

Figure 1. Chemical structure of *N*-(4-carboxyphenyl)trimellitimide dibutyl ester (NCTD).

Experimental Section

Synthesis. *N*-(4-Carboxyphenyl)trimellitimide was synthesized as described in refs 4 and 5. The dibutyl ester was prepared by solving the dichloride of *N*-(4-carboxyphenyl)trimellitimide (0.05 mol) and 0.1 mol butanol in 400 mL dichloromethane. A 0.1 mol portion of pyridine mixed with 50 mL dichloromethane was added dropwise. After stirring the mixture for 20 h at room temperature, it was washed with 1 N hydrochloric acid and three times with water. The solution was dried with sodium sulfate. After evaporating the solvent, the product was washed with petroleum ether and dried at 50 °C. For further purification, column chromatography was performed twice. The column was filled with silica gel; a mixture of petroleum ether and chloroform was used as an eluent. The amount of chloroform was increased from 25 to 100 vol.-%. The product was confirmed by ^{1}H- and ^{13}C NMR.

Fluorescence Measurements and UV Absorption Spectra. All the measurements of fluorescence and UV absorption spectra were performed on solutions of NCTD. The solvents used were cyclohexane, chloroform, and 1,1,1,3,3,3-hexafluoro-2-popanol

* Corresponding author. E-mail: spies@desy.de

10.1021/jp021560i CCC: $25.00
Published on Web 01/07/2003

(HFIP), all purchased from Merck with a degree of purity suitable for spectroscopy (UVASOL).

UV Absorption and Fluorescence Spectra. UV absorption spectra were measured by means of a Biochrom 4060 spectrometer from Pharmacia using quartz glass cells with 10 mm light path with respect to the pure solvent. Fluorescence spectra were measured by means of an Aminco SPF-500 spectrofluorometer. The diluted solutions were placed in quadratic quartz glass cells (light path 10 mm). The concentrated solutions were measured in triangle cells in transmission geometry. Excitation spectra were corrected with respect to a rhodamine B screen solution (3 g/L in ethylene glycol).

Time-Resolved Fluorescence Measurements. Time-resolved fluorescence measurements were performed at the beamline VISUV at the Hamburger Synchrotronstrahlungslabor HASYLAB at Deutsches Elektronensynchrotron DESY. The pulse width of the storage ring DORIS is about 150 ps (fwhm) with a repetition frequency of 2 or 5 MHz depending on the operation mode. The excitation light was monochromatized by a grating monochromator (Jobin Yvon type H10UV, bandwidth 16 nm). The luminescence light passed through a second monochromator (Jobin Yvon type H320, bandwidth 4 nm). In case of weak fluorescence intensity, a band-pass filter (bandwidth 40 nm) from Melles Griot was used instead of a second monochromator. Single photon counting detection was performed using a microchannel plate photomultiplier type R3809U-50 from Hamamatsu. The instrument response function was observed by scattering at milk (fwhm about 300 ps). The time interval between two adjacent data points was 49 ps. Fluorescence decay curves were recorded with at least 10 000 counts in the maximum channel. The diluted solutions were measured in quadratic quartz glass cells (light path 5 mm) and the fluorescence light was recorded perpendicular to the excitation light. The concentrated solutions were measured in triangular cells in transmission geometry. In this case, additionally a band-pass filter (band-pass 10 nm) was mounted after the first monochromator for stray light reduction. All measurements were carried out at 288 K. For data evaluation a least-squares fitting procedure with exponential functions was performed as described in ref 6.

Quantum Mechanical Calculations. The calculations were performed using the program HyperChem 6.02 from Hypercube. For ground-state geometry optimization the AM1 method[7,8] was used. The UV spectra and the orbitals of the optimized molecules were calculated with the ZINDO/S method[9,10] taking into account configuration interaction from HOMO-9 to LUMO+9.

Results and Discussion

To obtain information about electronic transitions in NCTD, generated by absorption of photons of different energy, first the UV absorption spectra will be interpreted. Figure 2 shows the UV absorption spectra of NCTD dissolved in cyclohexane, chloroform, and HFIP, concentration 10^{-5} M in cyclohexane and chloroform, 2×10^{-5} M in HFIP. The solvent HFIP was used because it is a good solvent for copoly(ester imides).[11] The absorption band observed around 310 nm is shown in a magnified representation on top of Figure 2. In this magnified view, a fine structure and a red shift with increasing solvent polarity is visible. For a better visibility of this fine structure in the magnified representation the measurements performed at 10^{-4} M concentration are shown for the solvents cyclohexane and chloroform.

The 310 nm absorption band can be attributed to electronic transitions of the trimellitimide or, as our calculations show, mainly to the trimellit moiety, i.e., the contribution of nitrogen is weak. This assignment as a local trimellit transition corresponds with measurements performed by Hasegawa et al.[12] who obtained for *N*-cyclohexylphthalimide dissolved in HFIP the lowest absorption band around 300 nm. The phthalimide transitions are comparable to the trimellitimide transitions. *N*-Cyclohexylphthalimide serves as a structure unit model compound for viewing the transitions of the phthalimide part of *N*-phenylphthalimide.[12] A comparison of the absorption spectra of *N*-phenylphthalimide with the two structure unit model compounds, i.e., *N*-cyclohexylphthalimide and *N*-phenylsuccinimide shows that the absorption spectrum of *N*-phenylphthalimide can be achieved by an additive overlay of the two lowest absorption bands of the two model compounds.[12] *N*-Phenylsuccinimide absorbs up to about 270 nm and *N*-cyclohexylphthalimide shows minimum absorption around 260 nm.[12] According to the additive overlay it can be concluded that the conjugation between the phthalimide moiety and the phenyl unit adjacent to the nitrogen is very small.[12] In connection with this observation we assume that the conjugation between the trimellit and the *N*-(4-carboxyphenyl) moiety is weak, too. This agrees with the quantum mechanical calculation presented in this paper. The assignment of the absorption around 310 nm to local transitions of the trimellit moiety is further supported by the results obtained by Gawronski et al.[13] On the basis of linear dicroism measurements, these authors showed that a comparable transition of phthalimide is observed around 300 nm and that it is a $\pi-\pi^*$ transition.[13]

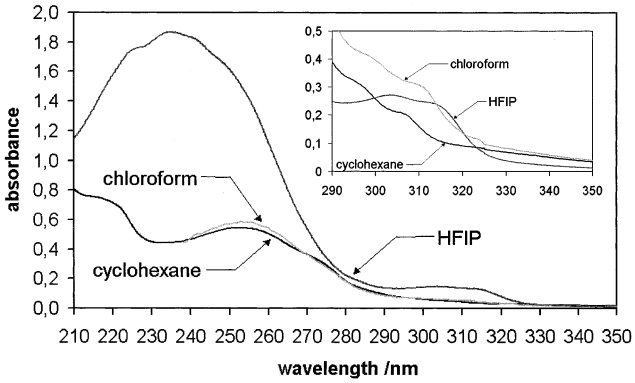

Figure 2. UV absorption spectra of NCTD dissolved in cyclohexane, chloroform, and HFIP, concentration about 10^{-5} M. In the magnified representation the concentration of the cyclohexane and chloroform solution is 10^{-4} M.

We conclude that the absorption blue-shifted to the 310 nm band arises from local transitions of the *N*-(4-carboxyphenyl) moiety. A comparison of the measured and the calculated UV absorption spectra supports these assumptions. The calculation of the UV absorption spectrum was performed with the ZINDO/S method.[9,10] Previously the geometry of NCTD was optimized with the AM1 method[7,8] in vacuum. A torsional angle of 28° between the plane of the trimellitimide moiety and the plane of the phenylene ring, i.e., a torsion around the C−N bond, was calculated. This value is in good agreement with the 30° torsional angle of the phenyl ring in *N*,*N*′-diphenylpyromellitimide obtained by LaFemina et al.[14] The optimized dihedral angle between trimellitimide and the phenylene ring is 180°. The optimization demonstrated a nitrogen sp^2 hybridization in the imide ring and coplanarity with the benzene ring of the trimellit moiety. For the calculation of the electronic configuration and the UV spectrum of NCTD with the ZINDO/S method a configuration interaction of the orbitals from HOMO-9 to LUMO+9 was taken into account. The calculated transitions

TABLE 1: UV Absorption Spectrum of NCTD Calculated Using ZINDO/S, C−N Torsional Angle 28°

λ/nm	orbitals	part of molecule	oscillator strength
318	HOMO → LUMO	*N*-(4-carboxy phenyl) → trimellit	0.009
289	HOMO-2 → LUMO+1	trimellit → trimellit	0.022
	HOMO-3 → LUMO	trimellit → trimellit	
282	HOMO → LUMO+4	*N*-(4-carboxy phenyl) → *N*-(4-carboxy phenyl)	0.007
	HOMO-1 → LUMO+2	*N*-(4-carboxy phenyl) → *N*-(4-carboxy phenyl)	
262	HOMO → LUMO+1	*N*-(4-carboxy phenyl) → trimellit	0.984
	HOMO → LUMO+2	*N*-(4-carboxy phenyl) → *N*-(4-carboxy phenyl)	
253	HOMO-1 → LUMO	*N*-(4-carboxy phenyl) → trimellit	0.039
252	HOMO-2 → LUMO	trimellit → trimellit	0.301
223	HOMO-2 → LUMO+1	trimellit → trimellit	0.942

are represented in Table 1. The participating orbitals and the absorption wavelengths are also given in Table 1 as well as a relation of the orbitals to the different parts of the molecule. This allocation to different parts of the molecule was made with regard to the observed maximum charge density of the calculated orbitals. The first transition obtained at 318 nm will be explained later on in this paper. The transition observed at 289 nm is localized on the trimellit part and the 282 nm transition is localized on the *N*-(4-carboxyphenyl) part. A direct relation of the transitions following at shorter wavelengths absorption bands to distinct parts of the molecule is not possible due to mixing of the participating orbitals and the small difference in the calculated wavelengths. The calculations show that the lowest transition observed at 223 nm is again caused by an almost pure trimellit transition. The overall shape of the spectrum is well described by this calculation, especially for the nonpolar solvent cyclohexane. Thus, it is concluded that the performed ZINDO/S calculation is very helpful to describe and interpret the measured absorption spectrum.

Now the first transition calculated at 318 nm will be interpreted. In the magnified representation of Figure 2 an absorption tail starting around 320 nm is visible. We suggest that this transition belongs to an intramolecular charge transfer (CT) transition from the *N*-(4-carboxyphenyl) moiety (electron donor) to the trimellit moiety (electron acceptor). The performed ZINDO/S and AM1 calculations corroborate this. Figure 3 shows the charge density of the HOMO and LUMO of NCTD. The HOMO electron density is mainly localized on the *N*-(4-carboxyphenyl) moiety. In contrast to this, the LUMO electron density is localized on the trimellit moiety, i.e., without including nitrogen. Thus, the HOMO−LUMO transition can be interpreted as a direct CT excitation by transferring an electron from the *N*-(4-carboxyphenyl) donor to the trimellit acceptor. The results of the calculation of the UV spectrum represented in Table 1 show that this transition is allowed and has a small oscillator strength in agreement with the weak measured absorbance. The calculated absorption wavelength is 318 nm, which corresponds with the onset of the absorption tail of the measurements performed in cyclohexane. As cyclohexane is a nonpolar solvent, the conformity with the calculated values in vacuum should be the best. For *N*-methylphthalimide, Gawronski et al.[13] also observed an absorption tail in the long wavelength region. Their quantum mechanical calculations and measurements show that in this case the absorption tail is generated by an $n-\pi^*$ transition.[13] As in our case a phenyl ring is adjacent to the nitrogen and the HOMO electrons are delocalized across the *N*-(4-carboxyphenyl) moiety, it should be denoted a $\pi-\pi^*$ transition.

Next the fluorescence emission and excitation spectra of NCTD dissolved in cyclohexane, chloroform, and HFIP ($c = 10^{-4}$ M) will be interpreted. The fluorescence spectra are shown in Figure 4. For comparison the respective UV absorption spectrum is also represented ($c = 10^{-5}$ M). The fluorescence

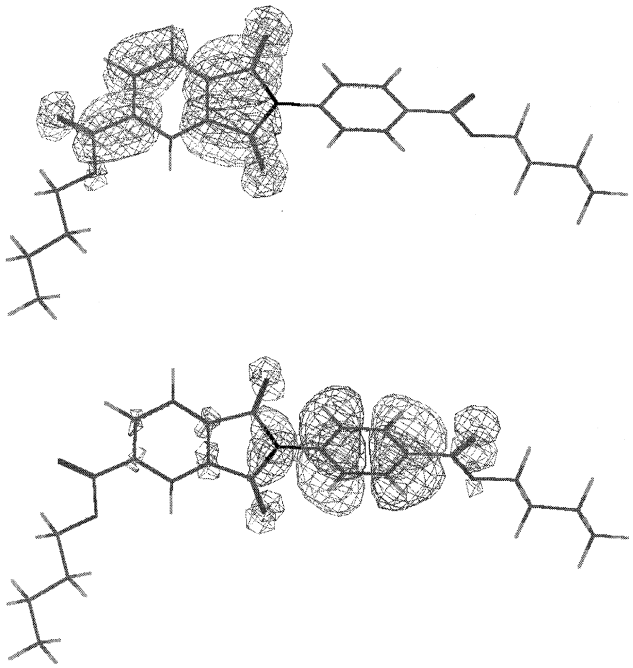

Figure 3. Charge density of LUMO (upper part) and HOMO (lower part) of NCTD using ZINDO/S calculation. The geometry was previously optimized using AM1, i.e., the C−N torsional angle is 28°.

spectra were measured at excitation wavelength $\lambda_{ex} = 290$ nm for cyclohexane, $\lambda_{ex} = 295$ nm for chloroform, and $\lambda_{ex} = 270$ nm for HFIP. A variation of the excitation wavelength up to about 310 nm has no influence on the observed spectra, i.e., the same spectrum was observed independent of the excitation wavelength. In all three solvents the fluorescence behavior is similar. A dominant red-shifted fluorescence band around 500 nm and a weak emission around 380 nm is visible. As two fluorescence bands appear, emission from two different excited states of the molecule exist. Normalization of the spectra was performed to obtain comparable fluorescence intensity values for the weak fluorescence band appearing around 380 nm and the excitation band observed around 310 nm. It is assumed that the weak fluorescence observed around 380 nm comes from the trimellit moiety.

Fluorescence excitation spectra shown in Figure 4 were measured in the emission range near the maximum intensity, i.e., at $\lambda_{em} = 500$ nm for cyclohexane, $\lambda_{em} = 500$ nm for chloroform, and $\lambda_{em} = 530$ nm for HFIP. As the excitation and UV-absorption spectra are very similar, excitation of the different parts of the molecule results in the same red-shifted emission. Thus, we conclude that different mechanisms or pathways must exist to form the excited state causing the red-shifted emission. Such a red-shifted emission is observed often when a charge transfer state is generated in the molecule.[2] As mentioned in the interpretation of the absorption spectra it is

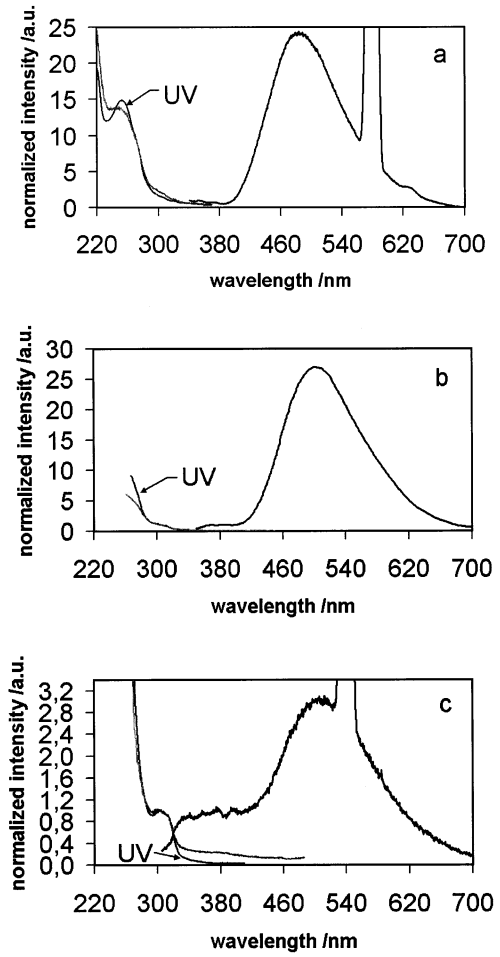

Figure 4. Fluorescence excitation and emission spectra of NCTD ($c = 10^{-4}$ M): (a) solvent cyclohexane, $\lambda_{em} = 500$ nm, $\lambda_{ex} = 290$ nm; (b) solvent chloroform, $\lambda_{em} = 500$ nm, $\lambda_{ex} = 295$ nm; (c) solvent HFIP, $\lambda_{em} = 530$ nm, $\lambda_{ex} = 270$ nm. The UV absorption spectra are also represented to enable comparison with the excitation spectra, respectively.

suggested that the lowest transition in energy is the CT transition from *N*-(4-carboxyphenyl) to trimellit, and the fluorescence of this state is assumed to cause the red-shifted band. As the same fluorescence spectra are observed by varying the excitation wavelength from about 250 to 310 nm, different ways of forming this CT species must exist. One way is the direct excitation at wavelengths longer than 310 nm. The cyclohexane and chloroform samples were excited at 330 nm and the red-shifted fluorescence band was recorded. In HFIP the fluorescence intensity in this excitation range was too weak at $c = 10^{-4}$ M to measure fluorescence spectra with reliable statistics. In addition, it is concluded that after excitation of the trimellit moiety (around 310 nm) an electron transfer takes place to form the CT state. This photoinduced electron transfer[15] will be explained in more detail in the next paragraph. The same fluorescence is observed after excitation of the *N*-(4-carboxyphenyl) moiety, i.e., exciting below 290 nm. The possible emission of *N*-(4-carboxyphenyl) should appear in the range of about 300 nm. Thus, this emission could be completely absorbed by or be transferred via excitation energy transfer[16] to the trimellit moiety where again electron transfer to the CT state could take place. Additionally, also in this case a photoinduced electron transfer can be imagined.

Now this electron transfer will be described in more detail. Figure 5 shows a schematically drawn electronic configuration

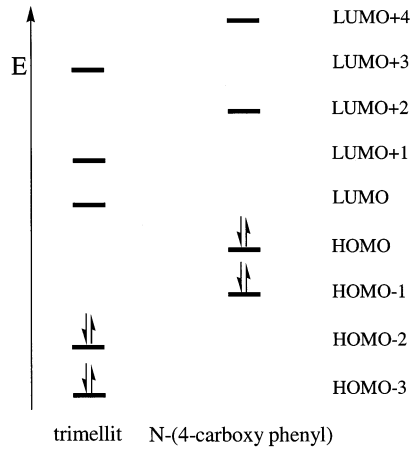

Figure 5. Electronic configuration of NCTD. The orbitals are assigned to different parts of the molecule in relation to maximum charge density.

of HOMO-3 up to LUMO+4. According to the calculated maximum of the electron density, the orbitals have been attached to the *N*-(4-carboxyphenyl) and the trimellit part of NCTD. It must be pointed out that this assignment is an approximation according to the nitrogen charge density. Often the charge density at the nitrogen is very weak and the LUMO+1 orbital shows a significant charge density on the nitrogen and is denoted as trimellit and not as trimellitimide orbital. Thus, when talking about the local transition of the trimellit moiety, it does not mean that influence of the neighbored nitrogen can be completely neglected. However, the main point is the assignment of nitrogen to the donor moiety in the CT transition as mentioned before. The connections of orbitals to the different parts of the NCTD-molecule that are shown herein have been compiled in Table 1 in conjunction with the calculated transitions. Illumination of the sample with light of wavelengths of about 310 nm leads to excitation of the trimellit moiety. According to Table 1, this transition is calculated to be observed at 289 nm in vacuum and is a mixed transition from HOMO-2 and HOMO-3 to LUMO and LUMO+1. Simplified, it can be assumed that one electron from HOMO-2 is transferred to LUMO, which can be recognized as a local transition of the trimellit in accordance to the electronic configuration shown in Figure 5. Now an electron transfer should take place from HOMO-1 and HOMO localized on *N*-(4-caboxyphenyl) to HOMO-2, and this results in single occupied HOMO and LUMO orbitals, i.e., the CT state. Such a transition was proposed by Hasegawa et al.[15] for *N*-(3-ethylphenyl)phthalimide and is called a photoinduced electron transfer. We suggest that it is comparable to the intermolecular exciplex formation proposed by Weller[17] as an electron is transferred from the donor to the excited acceptor. In our case an intramolecular CT is investigated, thus, it is suggested that this electron transfer can be compared to an internal conversion process. According to the electronic configuration shown in Figure 5 and in correlation to the exciplex formation,[17] also an electron transfer might take place from the excited donor to the acceptor. In this case a local excitation of the *N*-(4-carboxyphenyl) moiety leads to a single occupied HOMO and LUMO+2. This is again a simplification as the calculation gives a mixed transition, see Table 1. After excitation, an electron transfer from the LUMO+2 to LUMO+1 and then to LUMO might take place, and again the CT state is formed. This is another possible explanation why the red-shifted CT emission is always observed independent of the excitation wavelength.

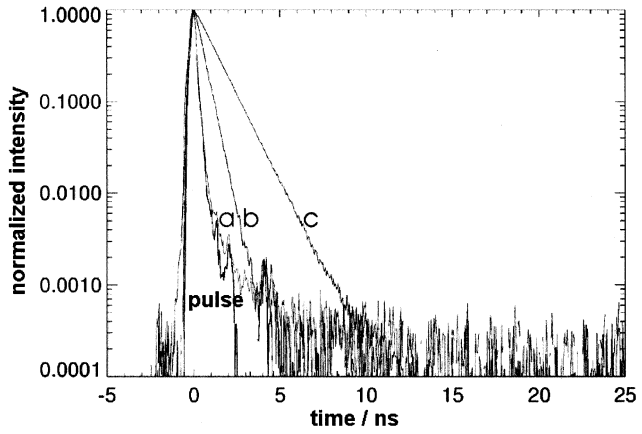

Figure 6. Time-resolved fluorescence decay curves of NCTD in 10^{-4} M solution: (a) solvent HFIP, $\lambda_{ex} = 270$ nm, $\lambda_{em} = 500$ nm; (b) solvent chloroform, $\lambda_{ex} = 280$ nm, $\lambda_{em} = 500$ nm; (c) solvent cyclohexane, $\lambda_{ex} = 280$ nm, $\lambda_{em} = 500$ nm. In addition, the instrument response function is represented, i.e., the scattered light pulse.

As an intramolecular CT state is formed we also have to discuss the influence of vibrational and torsional motions of the molecule. According to the observation of the dual fluorescence of amino benzonitrile derivatives, the influence of twisting around the C−N bond and of the nitrogen pyramidalization is discussed in connection with formation of the CT state.[18−20] The performed ZINDO/S calculation shows that in our case the CT state is the lowest in energy and can be excited directly. Thus, no promoting motion is necessary to explain the red-shifted emission. On the contrary, an increasing torsional angle or a pyramidalization of the nitrogen leads to a blue shift of the HOMO/LUMO transition (S_1), while the calculated second transition, i.e., the local excitation of the trimellit moiety, is unchanged (S_2). Thus, these motions do not explain an increasing red shift of the CT fluorescence but the internal conversion rate from S_2 to S_1 might be increased due to a decrease of the S_1 S_2 energy gap. We have to point out that the ZINDO/S calculations have been performed under vacuum conditions. In a polar solvent the more polar S_1(CT) state should be more red-shifted than the S_2 state which in contrast to the vacuum calculations increases the energy gap.

In addition, time-resolved fluorescence decay curves have been recorded. Figure 6 shows the fluorescence decay curves of NCTD dissolved in cyclohexane, chloroform, and HFIP ($c = 10^{-4}$ M). The emission was monitored at 500 nm, i.e., in the maximum range of the CT fluorescence. Variation of the excitation wavelength up to about 310 nm has no influence on the observed decay curves. Single exponential decays are measured in cyclohexane and chloroform solution. The calculated fluorescence decay times are 1.1 and 0.4 ns, respectively. Table 2 shows the parameters of fits to the decay curves using exponential functions. The decay in HFIP is too fast to be measured in this experiment. The measured curve is identical to the scattering pulse, which is also represented in Figure 6, consequently a fit of an exponential function to this curve leads to a poor χ^2 value. In Table 2, a 100 ps decay time is given for HFIP solutions which is only an approximation. It was confirmed that this short fluorescence lifetime is not caused by oxygen quenching. Bubbling nitrogen through the solution does not influence the decay behavior.

The probability of direct excitation of the CT state is small, as the measured and calculated UV absorption spectra show. Thus, the dominant mechanism of the CT state formation is a delayed one. Scheme 1 shows the proposed kinetics model of

TABLE 2: Parameters of Fits with Exponential Functions to the Decay Curves Shown in Figures 6, 8, and 9, $\lambda_{em} = 500 \pm 20$ nm

conc mol/L	solvent	λ_{ex} nm	τ_1 ns	A_1 %	τ_2 ns	A_2 %	τ_3 ns	A_3 %	χ^2	counts max. channel
10^{-4}	cyclohexane	280	1.1	100					1.1	20000
10^{-4}	chloroform	280	0.4	100					1.1	15000
10^{-4}	HFIP	270	0.1	100					2.3	18000
10^{-3}	chloroform	320	0.4	100					1.2	22000
10^{-1}	chloroform	370	0.4	99.9			3.4	0.1	1.5	14000
10^{-1}	chloroform	390	0.4	96.7	0.9	2.9	4.1	0.4	1.0	48000
10^{-1}	chloroform	400	0.4	92.4	0.9	6.7	4.2	0.9	1.2	17000
10^{-1}	chloroform	410	0.4	91.2	1.5	7.5	5.9	1.3	1.0	10000
10^{-1}	chloroform	430	0.5	73.7	2.3	21.9	6.7	4.3	1.5	10000
10^{-1}	HFIP	270	0.1	100					3.1	12000
10^{-1}	HFIP	300	0.1	100					6.7	21000
10^{-1}	HFIP	320	0.1	100					7.0	24000
10^{-1}	HFIP	340	0.1	99.7	0.8	0.2	4.9	0.1	0.8	29000
10^{-1}	HFIP	360	0.1	99.5	1.8	0.4	7.9	0.1	0.9	35000
10^{-1}	HFIP	370	0.1	98.5	2.2	1.2	9.3	0.3	1.3	13000
10^{-1}	HFIP	380	0.2	96.5	2.1	2.9	8.9	0.6	2.0	17000
10^{-1}	HFIP	390	0.1	92.7	2.1	6.1	8.8	1.2	1.2	17000
10^{-1}	HFIP	400	0.1	82.5	2.2	14.7	9.1	2.8	1.1	15000
10^{-1}	HFIP	410	0.1	63.5	2.2	30.7	9.0	5.7	1.1	14000

SCHEME 1

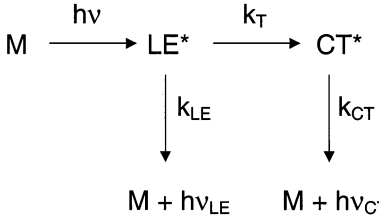

the delayed CT state formation. M is the molecule in the ground state. The local excited-state LE* represents the excited trimellit moiety or as discussed before it might also be the local excited *N*-(4-carboxyphenyl) moiety, CT* is the excited charge transfer state. Solving the differential equations describing the model one obtains

$$N_{LE}(t) = [LE^*]_{t=0} \exp(-t(k_{LE} + k_T)) \quad (1)$$

$$N_{CT}(t) = -A \exp(-t(k_{LE} + k_T)) + A \exp(-tk_{CT}) + [CT^*]_{t=0} \exp(-tk_{CT}) \quad (2)$$

$$A = \frac{k_T[LE^*]_{t=0}}{k_T + k_{LE} - k_{CT}}$$

where $N_{LE}(t)$ and $N_{CT}(t)$ are the number of excited molecules at time t. The formation rate constant of the CT state is denoted as k_T, while k_{LE} and k_{CT} are rate constants describing the radiative and nonradiative decay of the locally excited and the CT state, respectively. The amount of CT states directly excited by the incoming light pulse is denoted $[CT^*]_{t=0}$. As the fluorescence decay curves have been recorded in the wavelength range of the pure CT fluorescence, eq 2 should describe the measured curves. According to eq 2 an increase of the curves for short times, i.e., a time delayed maximum, is expected. Assuming that the rate constant k_T describes an internal conversion from S_2 to S_1, the time delayed CT* state formation is too fast to be detected by our experiment, and k_T^{-1} is expected to be in the ps range. A CT formation in the order of ps corresponds with Hasegawa et al.,[12] who estimated the rate of CT formation in aromatic polyimides to be larger than 5×10^{11} s^{-1}. The back-reaction to LE* is neglected as the CT state is lower in energy. This corresponds with the assumption of

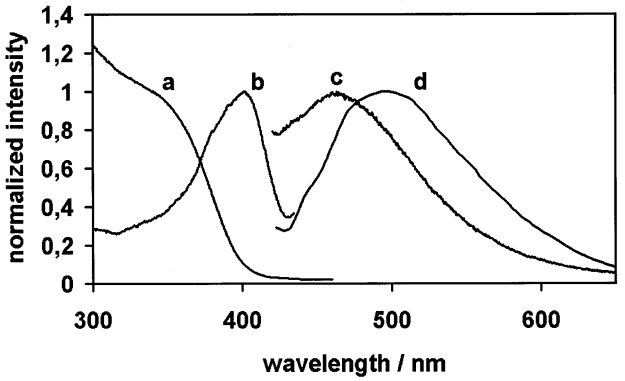

Figure 7. Fluorescence excitation and emission spectra of 10^{-1} M NCTD solutions: (a) solvent chloroform, $\lambda_{em} = 500$ nm; (b) solvent HFIP, $\lambda_{em} = 450$ nm; (c) solvent HFIP, $\lambda_{ex} = 410$ nm; (d) solvent chloroform, $\lambda_{ex} = 410$ nm.

CT state formation as an internal conversion process followed by vibrational relaxation. Thus, the decay time calculated from the measured curves represents the fluorescence lifetime of the CT state. The presence of a large transfer rate k_T from LE* to CT explains the weak fluorescence intensity of the LE state as shown in Figure 4, i.e., the weak emission obtained around 380 nm which is assumed to come from the trimellit moiety. The fluorescence intensity of the LE state was too weak to perform time-resolved measurements with reliable statistics in this emission range. The measured lifetimes of the CT in different solvents seem to be related to the polarity of the solvents. With increasing solvent polarity the fluorescence lifetime decreases. As the fluorescence is observed to shift toward red with increasing solvent polarity, the closer vicinity of the solvated excited state and respective solvated ground state might cause an increase of the nonradiative decay rates. In relation to this, the fluorescence intensity turns out to be the weakest in HFIP. Additionally, in HFIP the largest LE/CT ratio was observed in the fluorescence spectra. We conclude that the increase of the nonradiative depopulation of the excited CT state causes the comparably large amount of LE fluorescence.

Next the measurements performed on concentrated solutions in chloroform and HFIP will be presented. The solubility in cyclohexane is too poor to prepare concentrated solutions. Figure 7 shows the fluorescence excitation and emission spectra of 10^{-1} M NCTD solutions dissolved in HFIP and chloroform. The spectra are normalized to maximum intensity, except for spectrum a. Spectrum a is the excitation spectrum of the chloroform solution measured at emission wavelength 500 nm. It is normalized to 340 nm to allow better comparison with the other spectra. When increasing the concentration of NCTD in chloroform, the appearance of a shoulder in the long wavelength range is observed. The respective fluorescence emission spectrum is spectrum d shown in Figure 7. The chloroform sample was excited at 410 nm. Increasing the concentration of NCTD in chloroform from 10^{-4} M to 10^{-1} M leads to slight changes in the measured fluorescence spectra, only. When comparing spectrum d of Figure 7 ($c = 10^{-1}$ M) with the fluorescence spectrum shown in Figure 4 ($c = 10^{-4}$ M), just a broadening in the short wavelengths range is observed with increasing concentration. In the solvent HFIP the change of the fluorescence excitation and emission spectra with increasing concentration is more pronounced. The excitation spectrum b in Figure 7 was recorded at emission wavelength 450 nm. A maximum is observed around 410 nm. The respective fluorescence emission spectrum c was measured at excitation wavelength 410 nm. The maximum intensity is observed around 460 nm. Thus, increasing the NCTD concentration in HFIP from 10^{-4} M to 10^{-1} M leads to a blue shift of the maximum of the fluorescence spectrum of about 60 nm, which can be seen by comparing of the respective spectra represented in Figures 4 and 7. This shift can already be measured in 10^{-2} M solutions. We suggest that the change of the fluorescence excitation and emission spectra with increasing NCTD concentration can be explained by the existence of ground-state stable dimers. As the fluorescence spectrum of the 10^{-1} M HFIP solution is blue-shifted compared to the CT fluorescence spectrum observed in diluted solution, and as the direct excitation of the CT state and the dimers seem to be overlaid, it is concluded that the dimer in the excited state is less polar than the monomeric excited CT state.

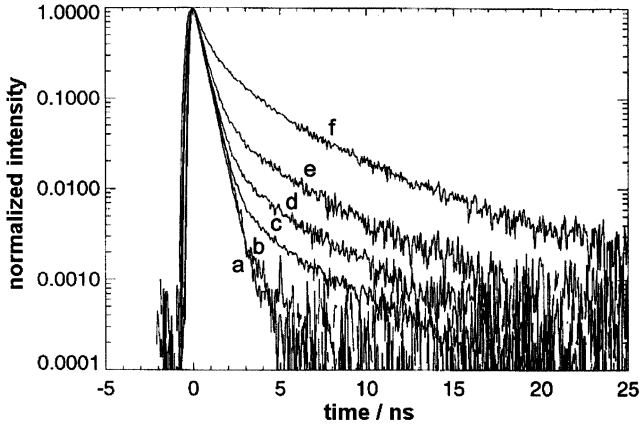

Figure 8. Fluorescence decay curves of NCTD in chloroform: (a) $c = 10^{-3}$ M, (b−f) $c = 10^{-1}$ M, $\lambda_{em} = 500$ nm; (a) $\lambda_{ex} = 320$ nm, (b) $\lambda_{ex} = 370$ nm, (c) $\lambda_{ex} = 390$ nm, (d) $\lambda_{ex} = 400$ nm, (e) $\lambda_{ex} = 410$ nm, (f) $\lambda_{ex} = 430$ nm.

To obtain more information about the ground-state stable dimer formation, time-resolved fluorescence measurements were performed. Figure 8 shows the fluorescence decay curves of NCTD dissolved in chloroform. The curves are normalized to their maximum. All curves were recorded at an emission wavelength of 500 nm. Curve a shows the fluorescence decay of a 10^{-3} M chloroform solution at $\lambda_{ex} = 320$ nm. Again, as already observed on the 10^{-4} M solution represented in Figure 6, a 0.4 ns decay time attributed to the CT emission was measured. Curves b−f were measured on the 10^{-1} M solution, the excitation wavelength was increased from 370 to 430 nm. At 370 nm excitation wavelength, the decay curve is almost identical to that observed for the CT emission. It is concluded that direct excitation of the CT state takes place at this wavelength. With increasing excitation wavelengths an increasing amount of species with longer decay times is observed, the 0.4 ns decay being present also. As the direct CT excitation is revealed in an absorption tail in the long wavelength range, the end of the range of possible direct CT excitation is not recognizable in the spectra. Thus, the observed 0.4 ns might still arise from direct excited CT species or from dimers with short lifetimes. The decay times and corresponding amplitudes calculated by fitting sums of exponential functions to the measured decay curves are presented in Table 2. We conclude that NCTD dimers exist which have longer lifetimes than the CT species, and an increasing amount of these dimers can be excited at longer wavelengths. The decays are multiexponential. The decay times given in Table 2 represent only mean values of an existing distribution of decay times.

A comparable change of the fluorescence decay curves with increasing excitation wavelength is observed with NCTD

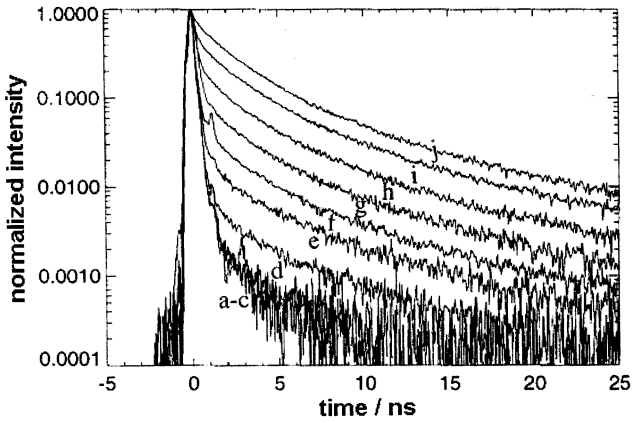

Figure 9. Fluorescence decay curves of NCTD in HFIP, $c = 10^{-1}$ M, $\lambda_{em} = 500$ nm: (a) $\lambda_{ex} = 270$ nm, (b) $\lambda_{ex} = 300$ nm, (c) $\lambda_{ex} = 320$ nm, (d) $\lambda_{ex} = 340$ nm, (e) $\lambda_{ex} = 360$ nm, (f) $\lambda_{ex} = 370$ nm, (g) $\lambda_{ex} = 380$ nm, (h) $\lambda_{ex} = 390$ nm, (i) $\lambda_{ex} = 400$ nm, (j) $\lambda_{ex} = 410$ nm.

dissolved in HFIP at concentration 10^{-1} M. The fluorescence decay curves are shown in Figure 9. All curves have been measured at emission wavelength 500 nm. Up to excitation wavelengths of 320 nm the decay curves look like those measured in 10^{-4} M solution, i.e., the fast CT decay is observed. From 340 nm upward an increasing amount of longer decay times is detected. The appearance of longer decay times happens at shorter excitation wavelengths in HFIP than in chloroform. Additionally, at the same excitation wavelength the amount of longer decay times is larger in HFIP than in chloroform. Thus, we conclude that the more polar solvent HFIP favors a ground-state stable dimer formation. The decay times and corresponding amplitudes are presented in Table 2.

A dimer is assumed to be a sandwich-like formation of two aromatic molecules which can be excited directly by the excitation light pulse in contrast to excimers which are formed by a diffusion-controlled mechanism of an excited molecule with a second one in the ground state.[21] The observed distribution of decay times gives reason to the assumption that different dimers exist. These dimers might be distinguishable according to the distance of the two molecules, or torsion, or a shift of one of the molecules.[22]

First AM1 calculations have been performed to obtain information about the geometry of the dimer. Therefore, two previously geometry optimized molecules, i.e., having a torsional angle of 28°, have been joined in a sandwich-like configuration. The starting distance was chosen to be 4 Å. For optimization of the head-to-head geometry one of the molecules was shifted cofacial by about 3 Å. This was done to increase the donor−acceptor interactions between the succinimide part and the phenylene ring of the opposite *N*-(4-carboxyphenylene) moiety and additionally between the carboxy groups and opposite rings.[1] The head-to-tail geometry was obtained by rotating one molecule 180° in plane. During the optimization the distance between the final methyl groups was held constant. The AM1 geometry optimization of the head-to-head geometry leads to a T-shaped dimer, i.e., one of the molecules turns nearly 90° around the long axis. In contrast, the head-to-tail geometry remains sandwich-like. Thus, it is concluded that the attractive forces between the two molecules are stronger in the head-to-tail geometry. The observed dimer conformations are shown in Figure 10. The torsion angle of 28° remains kept.

Additionally, ZINDO/S calculations were performed with the two dimers observed after the AM1 geometry optimization. We report only on the first two singulett transitions. In the case of the T-shaped head-to-head dimer, the calculated orbitals are localized on a single molecule. Thus, the two lowest transitions are comparable to the local CT transition observed for the single molecule. In contrast, for the head-to-tail dimer the ZINDO/S calculation shows that the pairs HOMO and HOMO-1 as well as LUMO and LUMO+1 have nearly the same energy, respectively. Both, HOMO and HOMO-1 are located on the *N*-(4-carboxyphenyl) part of both molecules simultaneously, just as LUMO and LUMO+1 are simultaneously located on the trimellit parts. Two degenerated mixed transitions are calculated to appear at 303 nm with oscillator strengths of 0.002 and 0.013. In analogy to the monomer, these transitions are CT transitions from both *N*-(4-carboxyphenyl) donors to the trimellit acceptors also. Thus, an intermolecular CT state is formed. According to the calculation, this dimer can be excited at shorter wavelengths than required for the direct CT excitation of the monomer which was calculated to be at 318 nm. This is in contrast to the performed time-resolved fluorescence measurements. We note in passing that only one single conformation under vacuum conditions was calculated. Variation of, e.g., the distance of the two molecules or a cofacial shift or a torsion of one molecule will shift the transition.[22] Thus, we conclude from the time-resolved fluorescence measurements that direct CT monomer excitation and dimer excitation take place in a comparable energy range and that different dimer conformations do exist. From the performed calculations we conclude that not only van der Waals forces[23,24] are responsible for the dimer formation of NCTD but also that additional attractive charge-transfer forces[25] are acting.

The performed calculations explain the blue shift of the dimer fluorescence compared to the monomer CT fluorescence. If the head-to-tail dimer is excited, an electron is transferred from both *N*-(4-carboxyphenyl) donors to both trimellit acceptors. In this head-to-tail geometry oppositely charged parts of the molecule face each other. We conclude that this CT dimer is less polar than the CT monomer, therefore, its emission arises blue-shifted compared to the monomer CT emission. This blue shift becomes clearly visible in the polar solvent HFIP. This dimer has CT

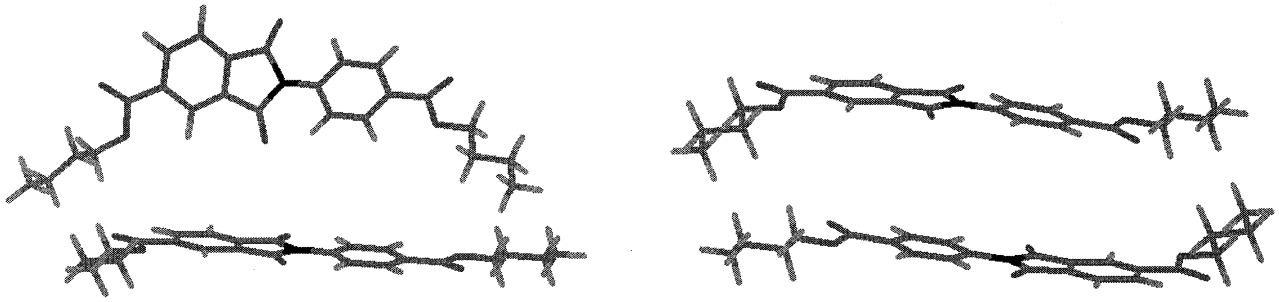

Figure 10. Dimer geometry obtained using AM1 geometry optimization. Left hand side, head-to-head dimer; right-hand side, head-to-tail dimer.

character, thus, it is a polar state. Polar states are better stabilized in polar solvents. Therefore, the dimer formation is favored in HFIP.

Conclusions

It is concluded that the absorption tail observed in the long wavelength range of the UV spectra represents the direct excitation of the intramolecular CT state. An electron is transferred from the *N*-(4-carboxyphenyl) moiety (donor) to the trimellit moiety (acceptor). Direct and indirect methods of intramolecular CT formation exist. To explain the indirect method of CT state formation, it is assumed that after excitation of the trimellit or the *N*-(4-carboxyphenyl) moiety an electron transfer takes place resulting in the excited CT state. The indirect method of CT state formation should be comparable to an internal conversion process. The rate constant of the CT formation is assumed to be in the ps range. With increasing concentration ground-state stable dimer formation is observed. The more polar solvent HFIP favors dimer formation. Attractive forces between sandwich-like conformations of two molecules are stronger in the head-to-tail than in the head-to-head geometry. The head-to-tail dimer has CT character. A mixed transition involving an electron transfer from both *N*-(4-carboxyphenyl) moieties to both trimellit moieties is calculated. This intermolecular CT state is less polar than the intramolecular CT, which relates to the blue shift of the dimer fluorescence band compared to the intramolecular (monomeric) CT band. As a distribution of decay times is observed from the time-resolved fluorescence decay curves, different dimers exist. They might be distinguishable due to the distance of the two molecules or of one of the molecules twisted or shifted relative to the other molecule.

Acknowledgment. We thank the Deutsche Forschungsgemeinschaft DFG for financial support under Contracts Sp 574/1-3 and 1-4.

References and Notes

(1) Kricheldorf, H. R.; Schwarz, G.; Domschke, A.; Linzer, V. *Macromolecules* **1993**, *26*, 5161.

(2) Hasegawa, M.; Horie, K. *Prog. Polym. Sci.* **2001**, *26*, 259.

(3) Kricheldorf, H. R.; Schwarz, G.; de Abajo, J.; de la Campa, J. *Polymer* **1991**, *5*, 943.

(4) de Abajo, J.; de la Campa, J.; Kricheldorf, H. R.; Schwarz, G. *Eur. Polym. J.* **1992**, *28*, 261.

(5) Kricheldorf, H. R.; Schwarz, G.; Nowatzki, W. *Polymer* **1989**, *30*, 937.

(6) Spies, C.; Gehrke, R. *Macromolecules* **1997**, *30*, 1701.

(7) Dewar, M. J. S.; Zoebisch, E. G.; Healy, E. F.; Stewart, J. J. P. *J. Am. Chem. Soc.* **1985**, *107*, 3902.

(8) Dewar, M. J. S.; Dieter, K. M. *J. Am. Chem. Soc.* **1986**, *108*, 8075.

(9) Ridley, J. E.; Zerner, M. C. *Theor. Chim. Acta* **1976**, *42*, 223.

(10) Bacon, A. D.; Zerner, M. C. *Theor. Chim. Acta* **1979**, *53*, 21.

(11) Spies, C.; Lorenc, A.; Gehrke, R.; Kricheldorf, H. R. *Macromol. Chem. Phys.*, submitted.

(12) Hasegawa, M.; Shindo, Y.; Sugimura, T.; Ohshima, S.; Horie, K.; Kochi, M.; Yokota, R.; Mita, I. *J. Polym. Sci.: Part B: Polym. Phys.* **1993**, *31*, 1617.

(13) Gawronski, J.; Kazmierczak, F.; Gawronska, K.; Rychlewska, U.; Norden, B.; Holmen, A. *J. Am. Chem. Soc.* **1998**, *120*, 12083.

(14) LaFemina, J. P.; Arjavalingam, G.; Hougham, G. *J. Chem. Phys.* **1989**, *90*, 5154.

(15) Hasegawa, M.; Sonobe, Y.; Shindo, Y.; Sugimura, T.; Karatsu, T.; Kitamura, A. *J. Phys. Chem.* **1994**, *98*, 10771.

(16) Förster, T. *Z. Naturforsch.* **1949**, *4a*, 321.

(17) Weller, A. *Pure Appl. Chem.* **1968**, *16*, 115.

(18) Rotkiewics, K.; Grellmann, K. H.; Grabowski, Z. R. *Chem. Phys. Lett.* **1973**, *19*, 315.

(19) Zachariasse, K. A.; Haar, T.; Hebecker, A.; Leinholos, U.; Kühnle, W. *Pure Appl. Chem.* **1993**, *65*, 1745.

(20) Gorse, A.-D.; Pesquer, M. *J. Phys. Chem.* **1995**, *99*, 4039.

(21) Birks, J. B.; Dyson, D. J.; Munro, I. H. *Prog. R. Soc. A* **1963**, *275*, 575.

(22) Cornil, J.; dos Santos, D. A.; Crispin, X.; Silbey, R.; Bredas, J. L. *J. Am. Chem. Soc.* **1998**, *120*, 1289.

(23) Gonzales, C.; Lim, E. C. *Chem. Phys. Lett.* **2000**, *322*, 382.

(24) Das, A.; Mahato, K. K.; Chakraborty, T. *J. Chem. Phys.* **2001**, *114*, 8310.

(25) Mulliken, R. S. *J. Am. Chem. Soc.* **1952**, *74*, 811.